How to cite: *Angew. Chem. Int. Ed.* **2025**, *64*, e202424493
doi.org/10.1002/anie.202424493

Lithium Metal Batteries

Machine Learning-Driven Mass Discovery and High-Throughput Screening of Fluoroether-Based Electrolytes for High-Stability Lithium Metal Batteries

Qingqing Jia[+], Hongguang Liu[+], Xueping Wang, Qiantu Tao, Lifeng Zheng, Junjie Li, Wei Wang, Ziteng Liu, Xu Gu, Tianyu Shen, Shaoyi Hou, Zhong Jin, and Jing Ma**

Abstract: Developing novel fluoroether electrolytes with high-voltage stability is an effective strategy to improve the performance of lithium metal batteries (LMB). However, the vast chemical space of fluoroether is underexplored due to the absence of effective tools to evaluate the potential used in high-voltage LMB. Herein, a framework was developed in combination of Voting ensemble algorithms and graph convolution neural network (GCNN), allowing the fast assessment of oxidative stability of non-aqueous liquid electrolytes, synthesizability of solvents as well as the solvation ability of them to dissolve lithium salts. Potential fluoroether solvent candidates for high-voltage LMB were screened out from a virtual library comprising 5576 electrolytes constructed by a combination of 1510 solvents and 4 salts. Among them, two fluorinated ethers, 1,1,1,3,3,3-hexafluoro-2-(2-methoxyethoxy) propane and 7,7,8,8-tetrafluoro-3,12-dimethoxy-2,5,10,13-tetraoxatetradecane, were successfully synthesized and showed satisfactory high-voltage stability, sufficient solvation ability and satisfactory cycling with almost 99.5 % coulombic efficiency in Li||NMC811 full cell. This work provided an efficient framework for the discovery of solvents with high-voltage tolerance in a vast structural space prior to experimental synthesis, accelerating the development of advanced electrolyte for high-energy-density rechargeable batteries.

Introduction

Elevating the energy density of lithium rechargeable batteries is urgently needed for future electric vehicles but is largely restrained by conventional electrolytes due to their limited voltage window (< 4.3 V) and severe side reactions on the high-voltage cathode surface.[1] Electrolyte engineering affords a promising approach to maximize the potential of high-voltage cathode. Benefiting from the strong electron-withdrawing effect of fluorine atoms, selective fluorination of carbon atoms in ethers to design single-salt-single-solvent electrolytes is one of the promising strategies for improving the performance of lithium metal battery (LMB) under high-voltage.[2] The sufficient ability for fluoroether to dissociate salts is the prerequisite to ensure mobile conductive ions but excessive solvation leads to bad outcomes as the formation of heavy Li^+ solvation cluster at the expense of slow ionic conductivity[3] and the weakening of de-solvation of the cations.[4] Several fluoroether solvents[5] in single-salt-single-solvent electrolytes possessing both oxidative stability and sufficient solvation for fast transport have been reported by fine-tuning the fluorinated position and fluorine content. Among these fluoroether solvents, the length of fluorinated alkyl segments and ether segments were varied in a modular fashion to systematic study of structure–property relationships and found that the positions and the amounts of fluorine greatly affect electrolyte performance. For instance, a family of fluorinated-1,2-diethoxyethanes with local polar $–CHF_2$ and fully fluorinated $–CF_3$ terminal substituent was reported and found that the $–CHF_2$ was an optimal group inducing higher ionic conduction and excellent electrode stability. Despite of the

[*] Q. Jia,[+] H. Liu,[+] X. Wang, Q. Tao, L. Zheng, J. Li, W. Wang, Z. Liu, X. Gu, T. Shen, S. Hou, Z. Jin, J. Ma
State Key Laboratory of Coordination Chemistry, MOE Key Laboratory of Mesoscopic Chemistry, Engineering Research Center of Photoresist Materials, Ministry of Education, MOE Key Laboratory of High Performance Polymer Materials and Technology, MOE Engineering Research Center of Photoresist Materials, Jiangsu Key Laboratory of Advanced Organic Materials, Tianchang New Materials and Energy Technology Research Center, Institute of Green Chemistry and Engineering, School of Chemistry and Chemical Engineering, Nanjing University, Nanjing, Jiangsu 210023, P. R. China
E-mail: zhongjin@nju.edu.cn
majing@nju.edu.cn

J. Ma
Key Laboratory of Mesoscopic Chemistry of Ministry of Education, School of Chemistry and Chemical Engineering, Nanjing University, Nanjing 210023, P. R. China

Z. Jin
State Key Laboratory of Coordination Chemistry, MOE Key Laboratory of Mesoscopic Chemistry, MOE Key Laboratory of High Performance Polymer Materials and Technology, Jiangsu Key Laboratory of Advanced Organic Materials, Tianchang New Materials and Energy Technology Research Center, Institute of Green Chemistry and Engineering, School of Chemistry and Chemical Engineering, Nanjing University, Nanjing, Jiangsu 210023, China

[+] These authors contributed equally to this work.

knowledge gained in these works, the structure space of fluoroether is extremely underexplored. In this work, we designed 5576 fluoroether-based single-salt-single-solvent electrolytes which are generated by randomly paired of 1394 fluoroether solvents and 4 lithium salts. The experimental investigation on such a vast structural space is impractical, leaving the chance of using machine learning (ML) as an alternative approach to accelerate the screening process.

ML-driven computational screening[6] has been applied to find molecules with certain redox potential suitable for flow batteries, the voltage of cathode materials and inorganic solid electrolytes that can inhibit the formation of dendrites in lithium metal anodes. A reliable framework to rapidly evaluate the two basic properties of non-aqueous liquid electrolytes, i.e., the experimental oxidation potential of liquid electrolytes and the dissolving capacity of solvents to lithium salts, is desired. Herein, we aim to propose a framework to rapidly screen promising fluoroether–based candidates possessing high-voltage stability and solvation ability as well as synthetic accessibility by combining the ML, synthetic accessibility scores (SAscore[7]), with the procedure of our framework shown in Figure 1. As the first step toward this goal, two interpretable ML model using the Voting algorithm were established to predict the experimental oxidation potential of nonaqueous liquid electrolyte and donor number (DN) values of solvents only based on 5 features, respectively. The solvents with high dissolving capacity to lithium salts were screened out with the values of DN[8] larger than 10 kcal/mol.[9] The deep learning model based on the graph convolution neural network (GCNN) architecture was also employed to achieve fast prediction of features with density functional theory (DFT) accuracy. The generalizability of these ML models was validated by the successful prediction of oxidation potential[10] and donor number published in literatures.[2,11]

In combination with the GCNN and ML models, the fast screening of promising solvents with high-voltage stability and reasonable solvation ability was implemented for the high-voltage lithium rechargeable batteries, two of which were randomly selected with relatively low SAscore, successfully synthesized, and subjected to electrochemical test in this work. The workflow ensures both effectiveness and convenience for the *in silico* discovery of promising novel fluoroether electrolytes from a huge chemical space, thus accelerating the development of Li rechargeable batteries with the high energy density.

Results and Discussion

Construction of Experimental Oxidation Potential Library

Despite various materials databases[12] are available, the specialized datasets focusing on the oxidation potentials of non-aqueous liquid electrolytes are rarely reported, which hinders the systematic development and optimization of electrolytes tailored for high-voltage applications. A dataset dedicated to the oxidative stability of electrolytes was constructed in this work and named LBSMox-ML. The primary objective in curating the LBSMox-ML dataset was to encompass a diverse range of solvents and lithium salts commonly employed in lithium-rechargeable battery electrolytes, including seven categories of organic solvents (esters, sulfoxides, carbonates, sulfites, ethers, sulfones, and benzene derivatives) and four lithium salt (lithium tetrafluoroborate ($LiBF_4$), lithium hexafluorophosphate ($LiPF_6$), lithium bis(fluorosulfonyl)imide (LiFSI), and lithium bis(trifluoromethanesulfonyl) imide (LiTFSI)), ensuring the structural diversity and representativeness of chemical space. The diversity of LBSMox-ML was achieved by including a wide spectrum of chemical environments, which is crucial for the generalizability of predictive models. More specifically, the LBSMox-ML is composed of 289 samples derived from three subsets, with their oxidation potential directly extracted from literatures (LBSMox-I, LBSMox-III) or determined by linear sweep voltammetry (LSV) measurement conducted in this work (LBSMox-II) (details in Table S1), with the details shown in Figure 2a, 2b. The wide ranges of elements (H, C, N, O, F, S, Cl and Br), atoms counts (5–125) and oxidation potential (2.5 V~7.0 V) (detail in Supporting Information) enhance the applicability of ML models in the broader chemical space. Among the LBSMox-ML dataset, conformations of molecules were taken into consideration using Molclus[13] software, with the computational details shown in Section S2. The LBSMox-ML data set was utilized to select important descriptors and establish a reliable ML model to predict the experimental oxidation potential of electrolyte. It should be noted that the present experimental oxidation potential library is an important supplement to the reported oxidation potentials calculated by theoretical calculations,[14] which are unsuitable for non-aqueous liquid electrolytes due to the neglect of the solvation environment effect in practice.

Collection of Donor Number Library

The DN[8] is an indicator of the Lewis basicity of solvents, which is one of the experimental parameters to gauge the dissolving capacity of solvents to lithium salts in the design of rechargeable battery electrolyte. The DN values of common solvents[15] were collected and named DN-ML dataset, which comprises 199 entries, with a wide distribution from 0 to 65 kcal/mol (Table S1, Figure S1). The DN-ML dataset was applied to construct ML models for the prediction of DN values of solvents.

Candidate Library

The establishment of a problem-orientated structure search space is crucial for the high-throughput screening of solvent candidates with satisfied properties. Prior knowledge learned from the known chemical space of high-performance fluoroether-based solvent of single-salt-single-solvent electrolytes[5,10] was used to guide the design of novel solvent molecules. These works demonstrated the feasibility of solvent design for high-voltage LMB by fluoride di-function-

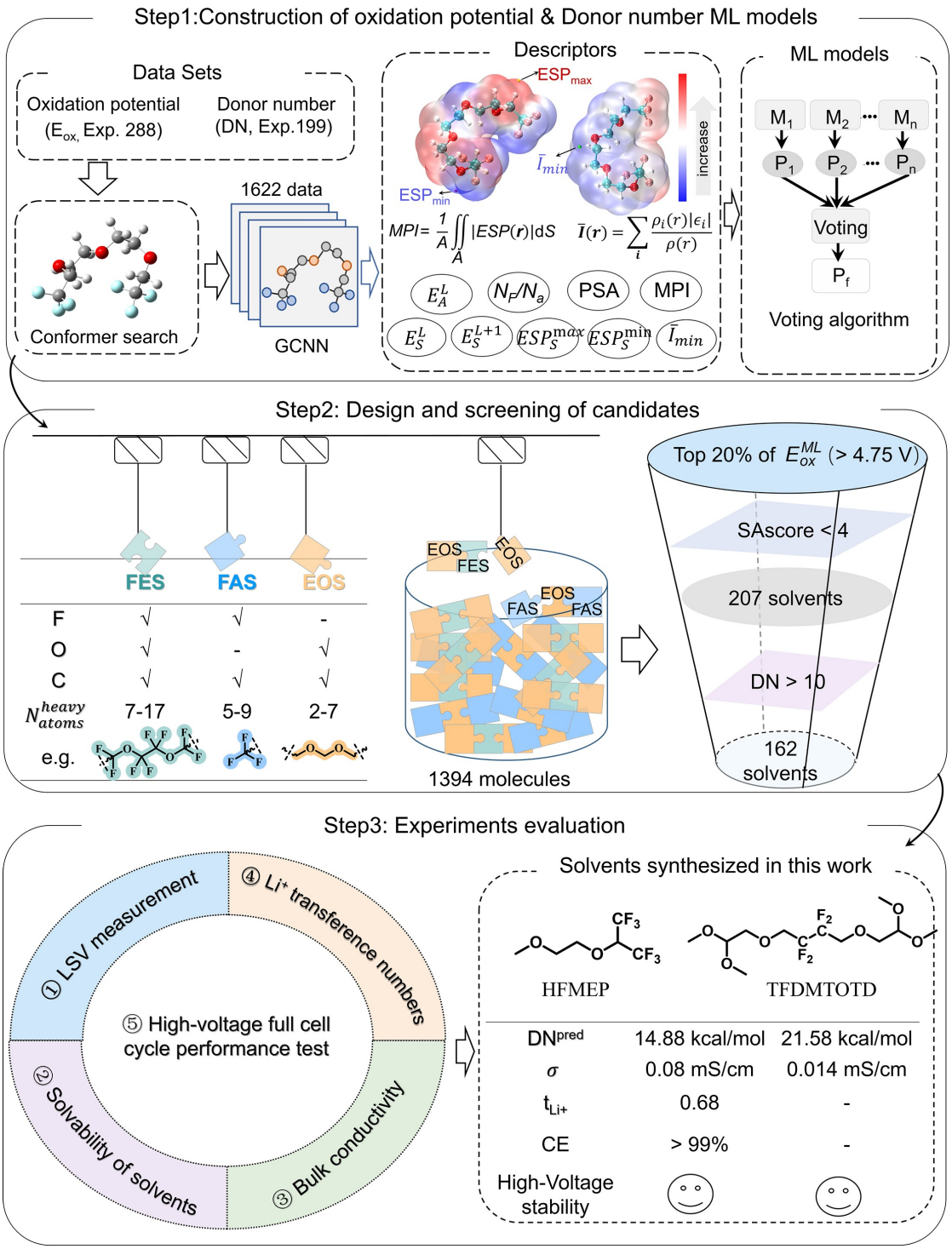

Figure 1. Workflow of electrolyte solvent screening for high-voltage Li metal batteries.

alized ether-based segments to manipulate solvent physiochemical properties (oxidative stability, ionic conductivity). Specifically, a serial of ethylene oxide segments (EOS) with different chain lengths was chosen as its good solvability of salts to ensure the reasonable conductivity of electrolyte molecules (Figure 2c). Meanwhile, two groups of fluorinated ethers (FES) and fluorinated alkyl segments (FAS) in different fluorination degree were introduced due to both the electron-drawing ability of fluorine, which could enhance the intrinsic oxidative stability of molecules, and the potential ability of the formation of LiF enriched solid electrolyte interface (SEI).[16] We systematically enumerated all the di-substituted species with sandwich configuration (FAS-EOS-FAS(847)/EOS-FES-EOS(663), Figure 2c),

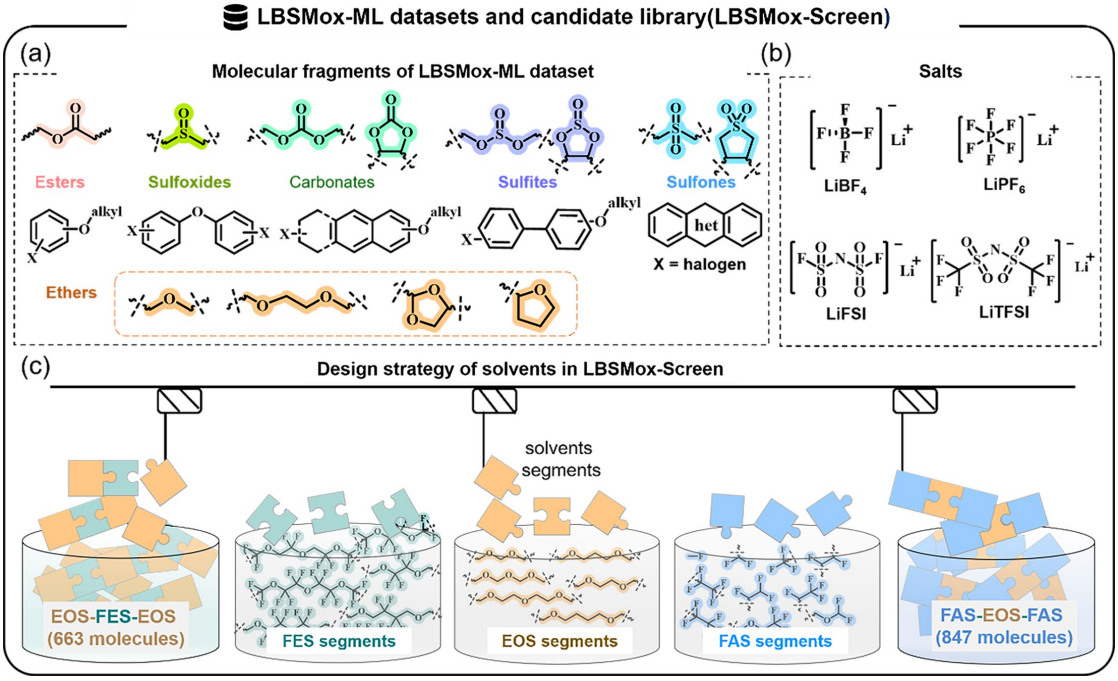

Figure 2. Illustrations of LBSMox-ML and LBSMox-Screen datasets.

which leads to a total of 1394 solvent candidates with promising high oxidation potential molecules. These solvents were paired with 4 lithium salts (Figure 2b) to generate 5576 electrolytes (LBSMox-Screen, Table S1).

Data Preprocessing and Model Building

Stratified sampling was applied in this work. The LBSMox-I data were divided into 8 groups (Table S2) based on the values of E_{ox}^{exp}. The DN-ML dataset was split into 6 groups (Table S3). Then, 80 % data from each group were randomly selected and combined as the training set, in which hyper-parameters were optimized by 10-fold cross-validated grid-search over a parameter grid space (details list in Tables S4 and S5) and the best hyper-parameters were searched out by evaluating the performance of the cross-validated model on the test set (Table S6). These best-hyperparameters were utilized for the construction of ML models with 10-fold cross-validation, covering seven ML algorithms: Support Vector Machines Regressor (SVM),[17] Gradient Boosting Regressor (GB),[18] Extra Trees Regressor (ET),[19] Decision Tree Regressor (DT),[20] Random Forest Regressor (RF),[21] and K-nearest Neighbours Regressor (KNN)[22] as well as the Voting ensemble approach (Voting) and two evaluation metrics: Mean Absolute Error (MAE) and Pearson's coefficients (r) were used to evaluate the performance of final models. The remaining 20 % data was served as the external test set which is invisible throughout the process of developing the ML models. All descriptors were scaled to 0–1 by the min/max scaler protocol (details in Section S3).

Feature Engineering for the Prediction of Oxidation Potential

The effect of the complicated electrolyte environment on the prediction of E_{ox}^{exp} was investigated. Total five species including the solvent···Li^+···anion (SLiA), solvent···Li^+ (SLi), and solvent···anion (SA) complexes, as well as the isolated solvents (S) and isolated anions (A) were constructed to simulate the solvated structures in electrolyte with low-cost. Three types descriptors related to electronic structure, polarity and geometrical parameters were computed and presented in Table S7 (details see Section S3). The importance of these species in predicting the oxidation potential was evaluated by feature elimination with the results shown in Figure S2. The solvent plays a dominant role in the prediction of E_{ox}^{exp}, as evidenced by the significant decrease in the performance of 7 ML models with the removal of descriptors stemmed from solvents (D_S) against all descriptors scheme. Similar but relatively weak influence of removal of SLi, SLiA and SA species on the performance was also found. Considering the cost to search for the interaction sites between the species to form SLiA, SLi and SA complexes, only the descriptors from the isolated solvent and anion species were further investigated.

The recursive feature elimination cross-validation (RFECV) approach was applied to reduce redundant features and enhance the interpretability of ML models (Figure S3). The RFECV approach automatically finds the optimal number of features and the best-scoring subset of features, which is beneficial for the feature selection in a vast feature space as usually the optimal feature number is unknown in advance. Twelve descriptors originated from the isolated solvents and isolated anions, denoted as D_{S+A}^{12}, were picked out from 26 descriptors (D_{S+A}^{26}) using the

RFECV approach with 10-fold cross-validation (Figure S3a, 3c). These D^{12}_{S+A} descriptors were further manually reduced to improve the interpretability and reduce redundancy, through integrating insights from the SHapley Additive exPlanations (SHAP) analysis, the Pearson correlation coefficient, and mutual information. The SHAP analysis provides interpretability by identifying the contribution of each feature to the model's output. The contribution of D^{12}_{S+A} descriptors for the oxidation potential conducted by the SHAP was shown in Figure S3b. The top five important descriptors are related to the electronic structure of the solvent, including the lowest unoccupied orbital energy level (LUMO) of solvents (E^L_S), the orbital energy levels adjacent to LUMO of the solvent (E^{L+1}_S) and the minimum value of average local ionization energy of the solvent ($\overline{I}_{min}$) which reveals the energy required to remove the least tightly-held electron[23] and is introduced as a guide to molecular reactivity,[24] the highest occupied orbital energy level (HOMO) of solvents (E^H_S), and the ratio of the number of F atoms to total atoms (N_F/N_a). Among them, N_F/N_a reflects the degree of fluorination of the fluoroether solvents molecule, which has been reported to have an impact on the oxidative stability of the electrolyte.[5b,c,25] The mutual information,[11b,26] which captures non-linear dependencies between features and the target, and the Pearson correlation coefficient for testing the linear relationships between the features were applied to identify the highly correlated features and potentially useful nonlinear information. The E^H_S, $\overline{I}_{min}$, E^{H-1}_S, E^{L+1}_S and E^L_S show dominant non-linear correlation with the E^{exp}_{ox}, as the mutual information shown in Figure S4a. The $\overline{I}_{min}$ are highly correlated with the E^H_S (r = −0.93) and E^{H-1}_S (r = −0.85), which was revealed by the Pearson correlation coefficient analysis with the results shown in Figure S3d. The high correlation between the $\overline{I}_{min}$ and E^H_S/E^{H-1}_S arises from the facts that (1) the $\overline{I}_{min}$ represents the energy required to remove the least tightly-held electron,[23] (2) E^H_S/E^{H-1}_S is associated with the electronic states of HOMO and HOMO-1, which contain the highest energy electrons that are most easily ionized. So as to reduce redundancy between the three descriptors ($\overline{I}_{min}$, E^H_S and E^{H-1}_S) only the $\overline{I}_{min}$ was retained for the establishment of ML models. The only anion-related descriptors, the LUMO energy level of anion (E^L_A), is reserved to reflect the effect of electrolyte environments, in which the influence of anion on the oxidative stability has been reported.[27] Finally, these top three descriptors (E^L_S, E^{L+1}_S, $\overline{I}_{min}$) together with the N_F/N_a and the LUMO energy level of anion (E^L_A) were screened and denoted as D^5_{S+A} (Table 1), which comprise the most important information with little information overlap and reflect the effects of different lithium salts on the oxidation potential (Figure 3a).

Seven ML models were generated on basis of the D^5_{S+A}, with the hyper-parameters listed in Table S6. Predictive performance metrics of these models on the 10-fold cross-validation set are shown in Figure 3b. Among these models, the Voting method composed by the GB, ET, and DT algorithms with a ratio of 6:9:1, shorted as GB-ET-DT, performs best and its excellent performance on the 10-fold cross-validation set was shown in Figure 3c ($r = 0.85 \pm 0.07$, $MAE = 0.30 \pm 0.03$ V). The performance of these models is comparable with the D^{12}_{S+A} descriptors scheme (Figure S5). The further removal of $\overline{I}_{min}$ and E^L_S, E^{L+1}_S yield a significant loss of accuracy with the wider distribution of error, shown in the violin plot (Figure 3d).

Accelerating the Calculation of DFT Descriptors by Graph Convolutional Neural Network

The GCNN was applied here to generate the key descriptors of $\overline{I}_{min}$ and E^L_S, E^{L+1}_Savoiding of DFT calculation and improving the applicability of ML models in numerous chemistry space for the E^{exp}_{ox} prediction. As one of the powerful deep learning architecture, GCNN has been widely used in the fast prediction of chemical properties, including the molecular polarity index,[28] formation energy[29] etc. A multilevel attention graph convolutional neural network (denoted as DeepMoleNet[30]) was developed in our group to predict 12 electronic structure properties (HOMO–LUMO gap, dipole moment, free energy, etc.) with outstanding performance. The 3 electronic structure properties ($\overline{I}_{min}$, E^L_S and E^{L+1}_S) among the D^5_{S+A} were predicted by GCNN with the hyper-parameters shown in Table S8. The 1622 data were split into training set, validation set and test

Table 1: Descriptors used in the oxidation potential and donor number prediction.

No.	Abbrev.	Description
The D^5_{S+A} used for oxidation potential prediction by the GB-ET-DT *model*		
1	E^L_S	Lowest unoccupied orbital energy level of solvents
2	E^{L+1}_S	Orbital energy levels adjacent to LUMO of solvents
3	$\overline{I}_{min}$	Minimum value of average local ionization energy of the solvent
4	N_F/N_a	The ratio of the number of F atoms to total atoms
5	E^L_A	Lowest unoccupied orbital energy level of anion
The descriptors used for donor number prediction by the SVM-DT-KNN model		
1'	$\overline{I}_{min}$	Minimum value of average local ionization energy of solvents
2'	ESP^{min}_S	Minimum value of electrostatic potential of solvents
3'	*PSA*	Polar surface area of solvents
4'	ESP^{max}_S	Maximum value of electrostatic potential of solvents
5'	*MPI*	Molecular polarity index of solvents

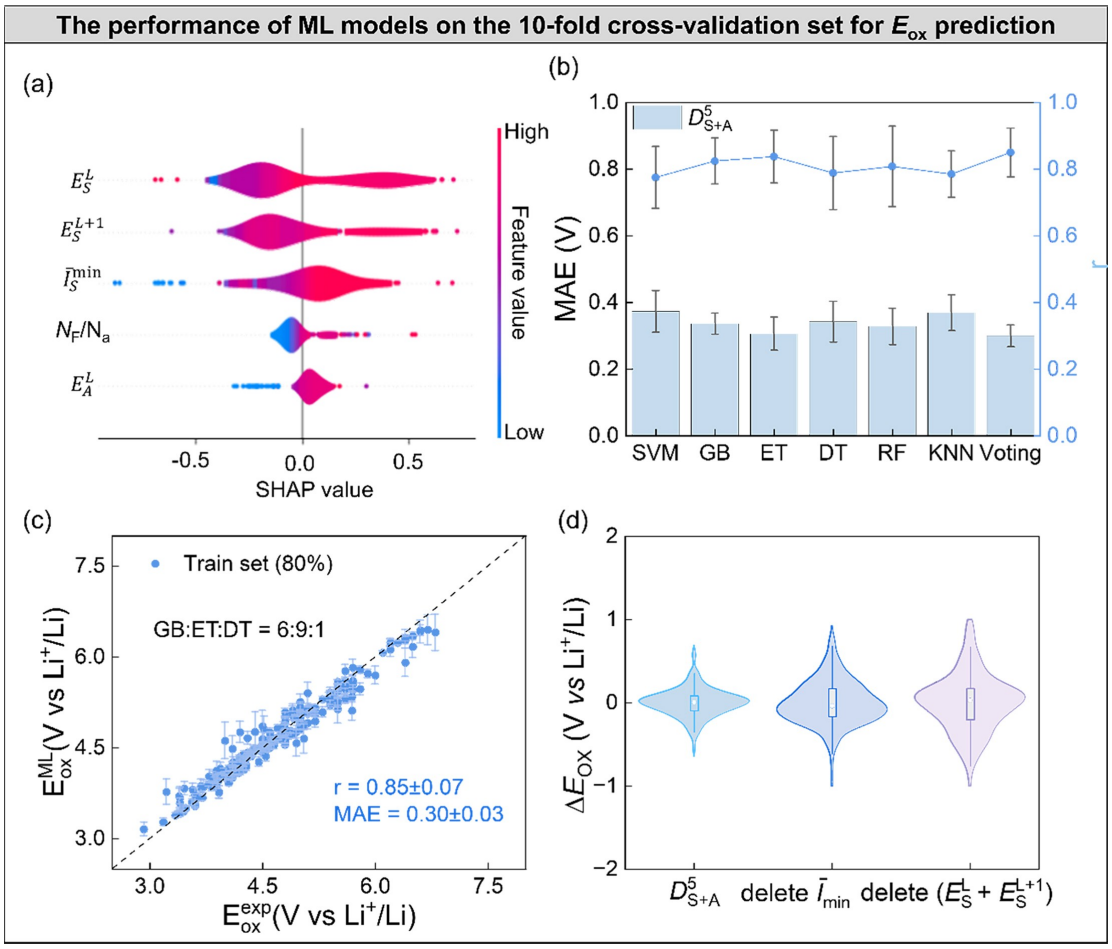

Figure 3. (a) The SHAP values of 5 descriptors (b) Performance of 7 ML model on the 10-fold cross-validation sets (228 samples) of LBSMox-ML dataset using D^5_{S+A} derived from solvent, and anion species; (c) The predicted oxidation potential of ML model trained by GB-ET-DT learners versus experimental oxidation potential on 10-fold cross-validation sets of LBSMox-ML dataset (d) The violet plot of the predicted errors (ΔE_{ox}) using GB-ET-DT learner based on D^5_{S+A} scheme and further removal of $\bar{I}_{min}$ and E_S^L, E_S^{L+1}. The error bars represent the standard deviation across the 10-folds.

set with 8:1:1, with the results shown in Figure S6. The predicted values for the average local ionization energy ($\bar{I}_{min}^{GCNN}$), the lowest unoccupied orbital energy level (E_L^{GCNN}) and the orbital energy levels adjacent to LUMO of the solvent (E_{L+1}^{GCNN}) by the GCNN correlated well with the values based on DFT calculations, with the r of 0.98, 0.98 and 0.93, as well as MAE of 0.07 eV, 0.02 eV, and 0.03 eV, respectively. Besides, the GCNN computational efficiency on the three descriptors ($\bar{I}_{min}$, E_S^L and E_S^{L+1}) significantly outperforms the DFT calculation, with the results shown in Figure S7. The GCNN only takes 2.04 seconds to complete the calculations of three descriptors on the 61 samples using 28 processors, while DFT takes 4999.90 seconds. Furthermore, the efficiency advantage of the GCNN method in calculating the above three descriptors is more prominent, when computing resources are limited (e.g. 14 processors).

The generalizability of the GCNN model on the prediction of these 3 electronic structure properties was further test on external test (61 molecules, external test set from LBSMox-ML data set) which is unseen in the training process of deep learning and not included in the GCNN data set (1622 data), with the results shown in Figure S6. The GCNN model shows satisfactory generalizability on the prediction of $\bar{I}_{min}$, E_S^L and E_S^{L+1} with the r of 0.97, 0.81 and 0.82, as well as MAE of 0.14 eV, 0.17 eV, and 0.11 eV, respectively. A few outliers led to large errors as their values are outside of the domain covered by the training data. For instance, the $\bar{I}_{min}^{DFT}$ value of the triethylenediami (TEDA) (8.66 eV) exceeds the range of training set (8.76–13.16 eV). Similarly, the E_L^{DFT} of 2,3-Dimethoxy-1,4-benzoquinone (DMBQ) (−2.43 eV) is out of the range of training data (−1.60–0.68 eV). These values predicted by GCNN models will be further used in the following section to test the potential of our framework combined with GB-ET-DT learners and GCNN in virtual screening of high-voltage solvents.

Generalizability Test of the GB-ET-DT Model

The effectiveness of D^5_{S+A} on the prediction of E^{exp}_{ox} of electrolytes was further tested on the external tests (Ta-

ble S9). As shown in Figure 4a, the GB-ET-DT learner performs well on the external test set composed of 61 electrolytes with diverse organic small molecules, including the ether, carbonate, ester, sulfone, sulfite and benzene derivatives, using D^5_{S+A} descriptors calculated by DFT ($\bar{I}^{DFT}_{min}$, E^{DFT}_L, E^{DFT}_{L+1}) with of 0.86 ± 0.01 and MAE of 0.32 ± 0.01 V. Similarly, the predicted E_{ox} values of GB-ET-DT learner ($E^{ML-GCNN}_{ox}$) using D^5_{S+A} descriptors calculated by GCNN ($\bar{I}^{GCNN}_{min}$, E^{GCNN}_L, E^{GCNN}_{L+1}) on the external test correlate well with the experiment (r = 0.84 ± 0.01, MAE = 0.33 ± 0.01 V, Figure S8). Most of the prediction errors of GB-ET-DT based on these 5 descriptors calculated by DFT or GCNN on the external test set are within E^{exp}_{ox} ± 0.5 V (Figure S9a), which falls within the range of experiment error. Four

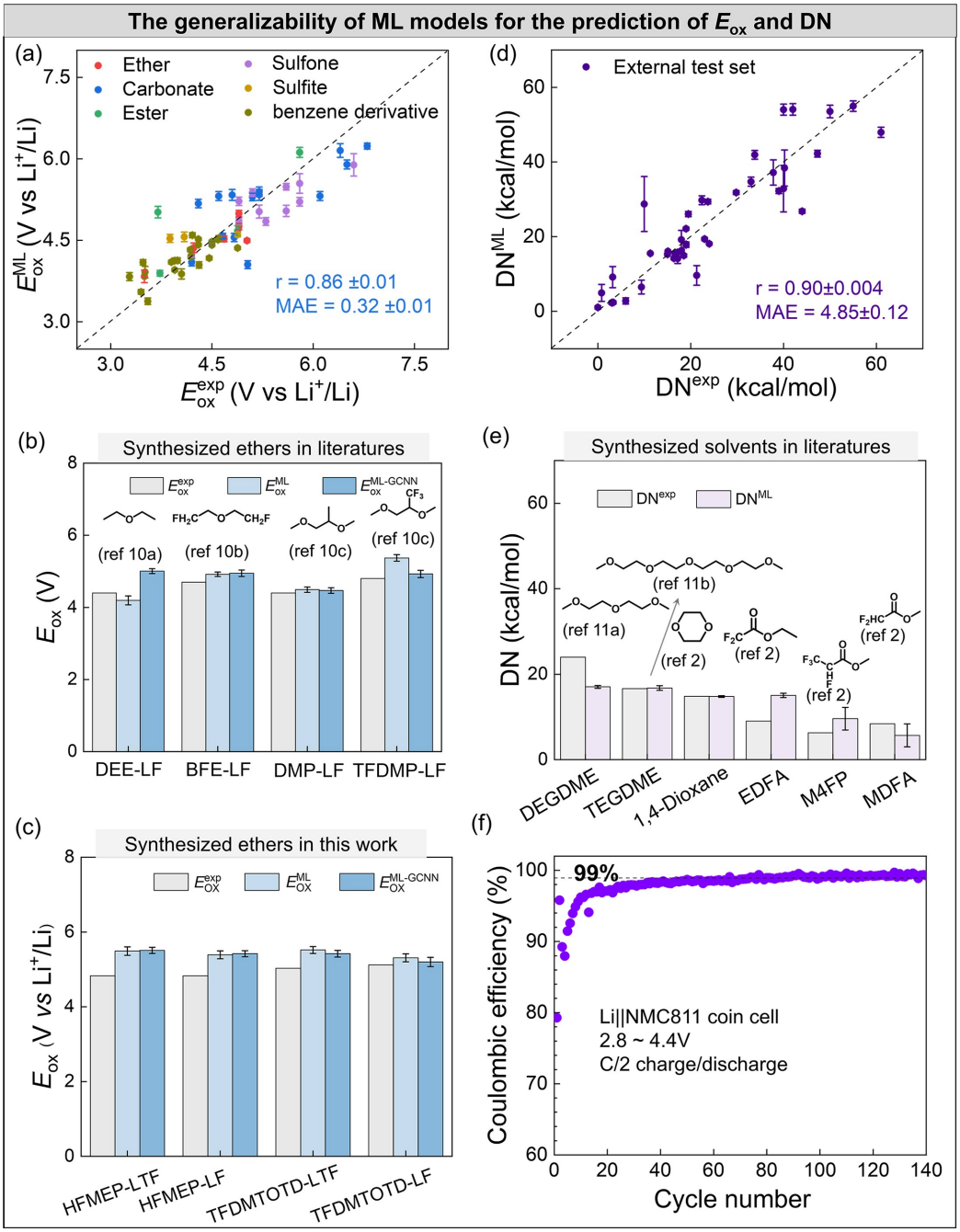

Figure 4. (a) The predicted oxidation potential of ML model trained by GB-ET-DT learners using D^5_{S+A} calculated by DFT ($\bar{I}_{min}$, E_L, E_{L+1}) and GCNN ($\bar{I}^{GCNN}_{min}$, E^{GCNN}_L, E^{GCNN}_{L+1}, results shown in parentheses) versus experimental oxidation potential on (a) external test sets (61 samples), (b) novel electrolytes solvents (DEE, BFE, DMP, and TFDMP) reported in latest literatures, and (c) fluoroether-based electrolytes synthesized in this work (d) the correlation of predicted donor number via SVM-DT-KNN learners versus the experimental DN values on external test sets of DN-ML (43 samples) and (e) on the 6 external tests molecules reported in the latest researches (f) galvanostatic cycling test of Li||NMC811 cells, using 1.5 M LiTFSI-HFMEP electrolytes at a current rate of C/2. The error bars represent the standard deviation across the 10-folds.

statistical methods, the t-test, Kolmogorov-Smirnov test, Mann-Whitney U test, and Pearson's correlation, were applied to assess the reliability of our model on external dataset, with the results shown in Table S10.

All tests support the statistical validity and robustness of the ML model on external datasets, confirming that there is no significant difference between the predicted and actual values. The Voting learner was further validated by the good prediction of oxidation potential of fluorinated/non-fluorinated ethers reported in the latest reports (Figure 4b), such as diethyl ether (DEE),[10a] bis(2-fluoroethyl) ethers (BFE),[10b] 1,2-dimethoxypropane (DMP),[10c] 1,1,1-trifluoro-2,3-dimethoxypropane (TFDMP).[10c] The $E_{ox}^{ML-GCNN}$ values are in qualitative agreement with the ML predicted values (E_{ox}^{ML}) based on D_{S+A}^{5} via DFT calculations and the values of E_{ox}^{exp} (Figure 4b). In conclusion, the good generalizability of GB-ET-DT learner on the above two external test sets demonstrates the potential of ML-GCNN framework on the prediction of E_{ox}^{exp} and virtual screening of potential high-voltage solvents in a vast chemical space.

Comparison with Other Methods

Two methods, the one is DFT-based thermodynamic cycle methods,[31] which was widely used to evaluate the oxidative stability, the other is RDKit descriptors[32]-based ML models, which has been successfully used in the prediction of oxidation potential DFT-based of homobenzylic ether molecules using RDKit descriptors,[33] were also utilized here to evaluate their ability on the oxidation potential prediction in such complex electrolyte systems and high-throughput screening of potential solvents with high-voltage tolerance from vast chemical space. As exemplified by the external test set which composed of 61 samples, the performance and computational costs were shown in Table 2, with the computational details given in Section S3. The DFT-based thermodynamic cycle methods ($r = 0.70$, $MAE = 0.94$) performs poor in the prediction of oxidation potential against the experiments on such complex systems, which is consistent with the findings that isolated species (solvents, anions) fail to capture the inherent oxidative stability of electrolytes, due to the neglect of interactions between solvents and anions.[27b,34] The weakening of oxidative stability of solvents in the presence of anions or other solvents has been demonstrated.[27] While DFT methods provide highly accurate predictions in idealized systems, their limitations in modeling complex electrolyte environments and their high computational cost make them less suitable for large-scale screening. The RDKit descriptors-based ML models ($r = 0.78 \pm 0.01$, $MAE = 0.40 \pm 0.01$) offer faster alternatives but struggle with capturing the essential interactions within electrolytes (Figure S10). In contrast, our ML model, the GB-ET-DT learners armed with D_{S+A}^{5} offers a promising solution by balancing both accuracy and computational efficiency, making it a superior tool for predicting the oxidation potential of electrolytes in lithium-rechargeable batteries. It should be noted that elucidating the oxidation potential prediction model remains a challenge as the multiple factors induced by electrode-electrolyte solid interface and the complex electrolyte composition.

Table 2: Comparison of the performance and computational cost between three methods for the prediction of oxidative stability on external test set ($n = 61$ samples). The error bars represent the standard deviation across the 10-folds.

	DFT-based	RDKit-based	GB-ET-DT(D_{S+A}^{5})
MAE	0.94	0.40 ± 0.01	0.34 ± 0.01
r	0.70	0.78 ± 0.01	0.86 ± 0.01
Computational cost[a](s)	9393.8	16.55	8.58

[a] Without considering time for geometry optimization, using 24 processors.

Donor Number Prediction

Five descriptors were selected by chemical intuition, namely the $\overline{I}_{min}$, polar surface area (PSA), molecular polarity index (MPI),[35] and the minimum value of electrostatic potential of solvents (ESP_S^{min}) as well as the maximum value of electrostatic potential (ESP_S^{max}) on the van der Waals (vdW) surface (Table 1). The detailed assessment of the SHAP values of these descriptors underlines the prominent role of $\overline{I}_{min}$ and ESP_S^{min} (Figure 5a), which is consistent with the results of mutual information (Figure S4b). The $\overline{I}_{min}$ and ESP_S^{min} are complementary for the description of intermolecular interaction.[36] The $\overline{I}_{min}$, which is defined as the lowest energy required to remove an electron from the molecules, reflects the polarization or charge transfer of molecules.[37] The ESP_S^{min} and ESP_S^{max} indicate the ability of molecules to interact electrostatically with Li^+ and anion of salts, respectively. As shown in Figure 5b, the samples with larger DN values are located at the left upper corner, characterized by the smaller values of $\overline{I}_{min}$ and larger values of the minus ESP_S^{min}, meaning the stronger electrostatic interaction between the solvents and Li^+ cations. The MPI is an indicator to gauche the molecular polarity and has been used in the prediction of lipophilicity.[28] The PSA defined as the surface belonging to polar atoms. We present a ML model for the theoretical prediction of DN values for candidate solvents to overcome experimental challenges and accelerate the discovery of novel electrolytes for Li rechargeable batteries, with the details shown in Section S3. As shown in Figure 5c, satisfactory ML models were developed using only five descriptors of solvents: $\overline{I}_{min}$, ESP_S^{min}, ESP_S^{max}, PSA and MPI. The Voting learner (SVM-DT-KNN = 4:8:3) performs best with 10-fold cross validation ($r = 0.92 \pm 0.05$, $MAE = 3.92 \pm 0.87$ kcal/mol, Figure 5d).

The generalizability of SVM-DT-KNN model on the prediction of DN values was further validated in the external test set (43 molecules) (Table S11). Most of the prediction errors of SVM-DT-KNN on the external test set are within DN ± 5 kcal/mol (Figure S9b). The predicted DN values (DN^{ML}) via SVM-DT-KNN model correlate well with the ones measured by experiments (DN^{exp}), with r of $0.90 \pm$

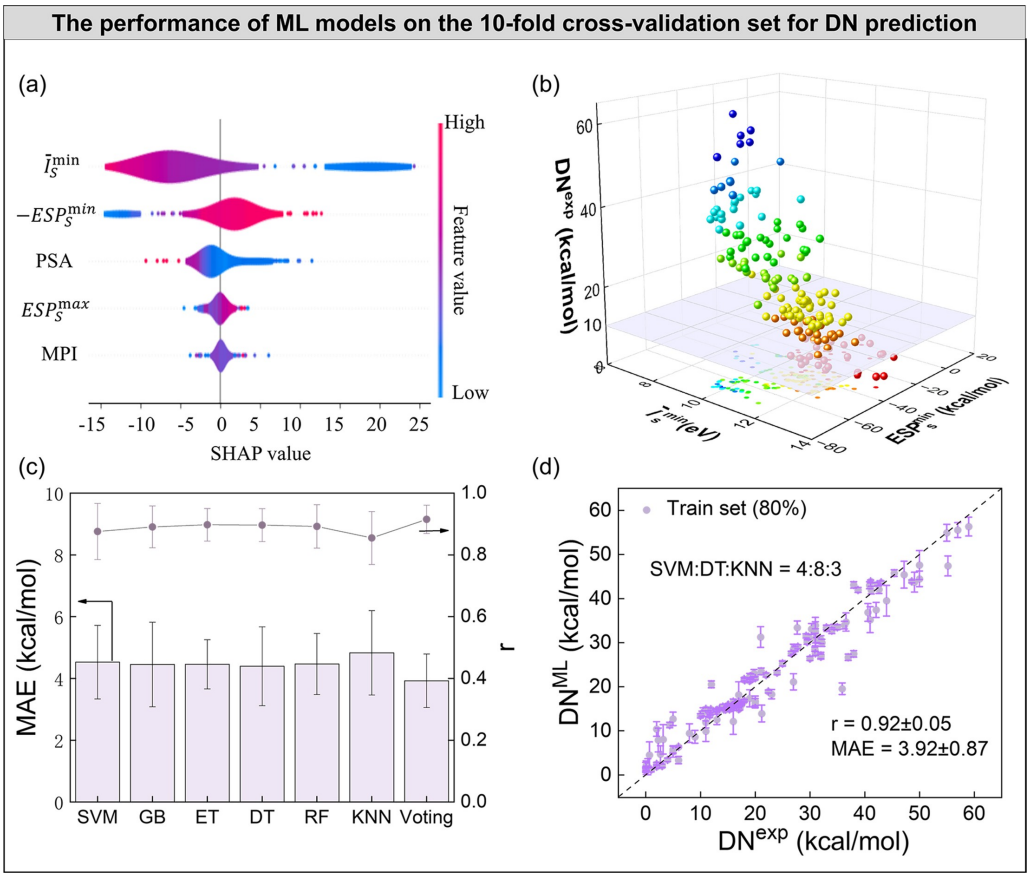

Figure 5. (a) The SHAP values of 5 descriptors; (b) the distribution of DN values measured by experiments and the values of the minimum value of average local ionization energy ($\bar{I}_{min}$) and the negative value of electrostatic potential minimum value of solvents (ESP_s^{min}) (c) performance of 7 ML models on the 10-fold cross-validation set (156 samples) (d) the experiment DN values versus the predicted DN values on the 10-fold cross-validation set using SVM-DT-KNN learner. The error bars represent the standard deviation across the 10-folds.

0.004 and MAE of 4.85 ± 0.12 (Figure 4d). Besides, this model was validated by the well prediction of DN values of 6 solvents in literatures, that is diethylene glycol dimethyl ether (DEGDME) collected from ComBat database,[11a] tetraethylene glycol dimethyl ether (TEGDME),[11b] 1,4-Dioxane (DO),[2] ethyl difluoroacetate (EDFA),[2] methyl 2,3,3,3-tetrafluoro propionate (M4FP),[2] and methyl 2,2-difluoro-2 (fluorosulfonyl)acetate (MDFA)[2] (Figure 4e).

Candidate Solvents Synthesized for High-Voltage LMB Electrolytes

The oxidative stability was first utilized to screen primary candidates. To this end, the well-performed GB-ET-DT model was employed here to predict the oxidation potential of LBSMox-Screen (Figure S9c), and the top 20 % of those were pre-screened as the candidates′ library, which comprises 1115 electrolytes consisting of 327 solvents and 4 salts ($LiBF_4$, $LiPF_6$, LiTFSI, LiFSI). The synthesizability of these solvents is further evaluated based on the SAscore developed by Ertl and Schuffenhauer[7] using RDKit library, which combines fragment contributions with a complexity penalty to provide a score ranging from 1 (very easy to synthesize) to 10 (very difficult to synthesize), with the computational details in Section S3. The solvents with SAscore < 4 were further screened. The DN values of these solvents were then calculated based on the SVM-DT-KNN model to evaluate their ability to dissociate Li salts, with the DN values ranging from 2 to 22 kcal/mol (Figure S9d).

Finally, 162 solvents, which possess high electrochemical stability and synthetic accessibility as well as adequate solvation (DN > 10 kcal/mol), were recommended to be promising solvent candidates used in high-voltage electrolytes (Table S12). Among these candidates, two fluorinated ethers, i.e., 1,1,1,3,3,3-hexafluoro-2- (2-methoxyethoxy) propane (HFMEP, DN = 14.88 kcal/mol) and 7,7,8,8-tetrafluoro-3,12-dimethoxy-2,5,10,13-tetraoxatetradecane (TFDMTOTD, DN = 21.58 kcal/mol), were synthesized in an economic way. These solvents were paired with four lithium salts (LiFSI, LiTFSI, $LiBF_4$, and $LiPF_6$) to generate electrolytes. Among these four lithium salts, LiTFSI (LTF) and LiFSI (LF) are prevalently applied in single-salts-single-solvent electrolytes based on fluorinated ethers solvents and exhibit superior solubility compared with $LiPF_6$ (LPF) and $LiBF_4$ (LBF). As expected, LiFSI and LiTFSI are more easily dissolved compared to $LiBF_4$ and $LiPF_6$, and can form high-concentration electrolytes (e.g. 2 M) in both HFMEP

and TFDMTOTD (Figure S11). The $LiPF_6$ could not fully dissolved in both the above two solvents at 1 M. The $LiBF_4$ completely dissolved in TFDMTOTD whereas its solubility in HFMEP is so poor that even a 1 M electrolyte cannot be achieved. This significant difference of solvent dissolving salts is consistent with the DN values of solvents predicted by SVM-DT-KNN model.

The electrochemical properties including the oxidative stability, bulk ionic conductivity and lithium-ion transference numbers (t_{Li+}) of electrolytes were measured with the details shown in Section S4. The electrolyte stability at high voltage was investigated by LSV measurements (Figure S12). The leakage current evolution of HFMEP and TFDMTOTD electrolytes with four lithium salts at conventional salts concentration (at 1 M) under a high-voltage scan indicates the reasonable high-voltage stability of these electrolytes except for the HFMEP-LF-1M. The anodic stability of electrolytes is influenced by the concentration of salts. Taking LiTFSI as an example, the increase of LiTFSI concentration significantly leads to the enhanced oxidative stability of HFMEP-LTF and the oxidation potential up to 4.83 V at 2 M (Figure S12). The ML models show the reasonable prediction of oxidative stability of electrolytes against the results of LSV, both using the descriptors obtained by DFT calculations or GCNN prediction (Figure 4c). Then the bulk conductivity(σ) and t_{Li^+} of these electrolytes were measured and shown in Figure S13, Figure S14, respectively. All HFMEP-LTF electrolytes at three concentrations possess relatively high t_{Li+} (>0.68) value and relative low conductivity at room temperature (less than 0.09 mS/cm). The applicability of HFMEP-LTF-1.5 M electrolyte under high-voltage full cell was further evaluated. The Li||NMC811 ($LiNi_{0.8}Mn_{0.1}Co_{0.1}O_2$) cell was assembled with the HFMEP-LTF-1.5 M electrolyte. The full cell cycled between 2.8 and 4.4 V *vs* Li^+/Li at a current rate of C/2 with almost 99.5 % Coulombic efficiency obtained at least 100 cycles (Figure 4f, Figure S15). The Coulombic efficiency is a key parameter to evaluate charge utilization and electrochemical reversibility of secondary batteries. The high Coulombic efficiency realized by the as-synthesized solvent demonstrates its promising potential for practical battery applications. First, it indicates minimal side reactions during the charge–discharge processes, which is crucial for maintaining battery capacity and extending battery lifespan. Second, the stability of the electrolyte-electrode interface, likely facilitated by the formation of a stable SEI layer, contributes to the high Coulombic efficiency. This stability is essential for the safe and reliable operation of high-voltage lithium metal batteries. Third, the stability of the solvent under high-voltage conditions suggests their potential for use in advanced battery systems requiring high-voltage cathodes. The high Coulombic efficiency demonstrates that the ML models hold significant potential for the discovery of novel fluoroether electrolytes with high-voltage stability.

Furthermore, the scalability of the synthesis process is a critical factor for practical applications and was needed further assessment in future. Preliminary investigations suggest that the synthesis routes are feasible, associated with relatively low costs (Table S13) and limited environmental impacts (Table S14). The environment toxicity of the two novel fluoroethers solvents was assessed by the comprehensive eco-toxicity indicators, including aquatic toxicity, bioaccumulation potential, and persistence in the environment, which are critical for assessing the long-term environmental risks of these solvents, using the Ecological Structure Activity Relationships (ECOSAR) Class Program,[38] with the results shown in Table S14. The HFMEP shows moderate environmental toxicity, with ChV values of 22.96 mg/L (Daphnia) and 39.36 mg/L (Green Algae) indicating that prolonged exposure could pose significant long-term risks to aquatic ecosystems, particularly to plants and invertebrates. The relatively high LC50 and ChV values for the TFDMTOTD suggest a lower environmental risk, particularly with respect to acute and chronic exposure in aquatic ecosystems. The environmental risks posed by themselves or their degradation products could potentially be mitigated through the recovery of fluoroethers using physical and chemical methods. It should be noted that the framework established in this work is not limited in screening fluorinated molecules but is scalable to the screen of non-fluorinated molecules to assess their oxidative stability, synthesizability and solvation power. Moving forward, we will incorporate the potential toxicity profiles of solvents into the design and screening of next-generation electrolytes, ensuring both performance and environmental sustainability.

Conclusions

A ML-driven workflow was developed to enable the rapid assessment of the high-voltage stability of electrolytes and solvation ability of solvents to dissolve lithium salts. A data set named LBSMox containing 5865 samples was constructed for the prediction of experimental oxidation potential of electrolytes. Two interpretable ML model armed with only 5 descriptors to assess the oxidation potential of electrolytes ($\bar{I}_{min}$, E_S^L, E_S^{L+1}, N_F/N_a and E_A^L) and the DN values ($\bar{I}_{min}$, ESP_S^{min}, ESP_S^{max}, PSA and MPI) were established, respectively. The generation of three DFT descriptors of solvents was accelerated by using GCNN with satisfactory accuracy. The generalizability of ML models was tested on the external test sets with good performance. High-throughput screening of promising solvents with high-voltage stability was performed. Two new fluorinated-ethers were synthesized in this work and subjected to experimental tests. Their potential application in high-voltage LMB was characterized by the LSV measurement and the good Coulombic efficiency of Li||NMC811 full cell. The deep learning-assisted interpretable machine learning models ensure both effectiveness and convenience for the discovery of promising fluoroether solvents with high-voltage stability from a huge chemical space, accelerating the development of Li rechargeable batteries with high energy density.

Author contributions

Jing Ma and Qingqing Jia initiated the project and the latter carried out the theoretical calculation. Qingqing Jia, Hongguang Liu, Lifeng Zheng, Qiantu Tao, Tianyu Shen, performed the measurements of electrochemical experiments. Qingqing Jia, Xueping Wang, Wei Wang and Junjie Li constructed the dataset and carried out the MD simulation. Qingqing Jia, Ziteng Liu, Xu Gu and Shaoyi Hou contribute to the codes for ML, GCNN and molecular generation, respectively. Zhong Jin guides the experiments. All authors contributed to the discussion of the results as well as the writing and revision of the manuscript.

Acknowledgements

This work was supported by the National Key Research and Development Program of China (2023ZD0120700), the National Natural Science Foundation of China (22033004, 22373049, 22479074 and 22475096), the Natural Science Foundation of Jiangsu Province (BK20232012, BK20240400 and BK20241236), the General Project of the Joint Fund of Equipment Pre-research and the Ministry of Education (8091B02052407), the Scientific and Technological Innovation Special Fund for Carbon Peak and Carbon Neutrality of Jiangsu Province (BK20220008), the Scientific and Technological Achievements Transformation Special Fund of Jiangsu Province (BA2023037), the International Collaboration Research Program of Nanjing City (202201007 and 2022SX00000955), the Gusu Leading Talent Program of Scientific and Technological Innovation and Entrepreneurship of Wujiang District in Suzhou City (ZXL2021273), and the Chenzhou National Sustainable Development Agenda Innovation Demonstration Zone Provincial Special Project (2023sfq11). We are grateful to the High Performance Computing Centre of Nanjing University for providing the IBM Blade cluster system and Bideparam for the help of compound synthesis. Thanks to Guoqiang Wang and Jiawei Chen from Nanjing University for their helps in experiments and data statistics.

Conflict of Interest

There are no conflicts to declare.

Data Availability Statement

The data that support the findings of this study are available from the corresponding author upon reasonable request.

Keywords: donor number · fluoroether electrolytes · high-voltage stability · high-throughput screening · machine learning

[1] E. Markevich, G. Salitra, Y. Talyosef, U. H. Kim, H. H. Ryu, Y. K. Sun, D. Aurbach, *ACS Appl. Energ. Mater.* **2018**, *1*, 2600–2607.
[2] J. J. Xu, J. X. Zhang, T. P. Pollard, Q. D. Li, S. Tan, S. Y. Hou, H. L. Wan, F. Chen, H. X. He, E. Y. Hu, K. Xu, X. Q. Yang, O. Borodin, C. S. Wang, *Nature* **2023**, *614*, 694–700.
[3] N. N. Rajput, X. H. Qu, N. Sa, A. K. Burrell, K. A. Persson, *J. Am. Chem. Soc.* **2015**, *137*, 3411–3420.
[4] T. Ma, Y. X. Ni, Q. R. Wang, W. J. Zhang, S. Jin, S. B. Zheng, X. Yang, Y. P. Hou, Z. L. Tao, J. Chen, *Angew. Chem. Int. Ed.* **2022**, *61*, e202207927.
[5] a) Z. Yu, P. E. Rudnicki, Z. Zhang, Z. Huang, H. Celik, S. T. Oyakhire, Y. Chen, X. Kong, S. C. Kim, X. Xiao, H. Wang, Y. Zheng, G. A. Kamat, M. S. Kim, S. F. Bent, J. Qin, Y. Cui, Z. Bao, *Nat. Energy* **2022**, *7*, 94–106; b) Z. Yu, H. Wang, X. Kong, W. Huang, Y. Tsao, D. G. Mackanic, K. Wang, X. Wang, W. Huang, S. Choudhury, Y. Zheng, C. V. Amanchukwu, S. T. Hung, Y. Ma, E. G. Lomeli, J. Qin, Y. Cui, Z. Bao, *Nat. Energy* **2020**, *5*, 526–533; c) P. Y. Ma, P. Mirmira, C. V. Amanchukwu, *ACS Cent. Sci.* **2021**, *7*, 1232–1244.
[6] Z. Ahmad, T. Xie, C. Maheshwari, J. C. Grossman, V. Viswanathan, *ACS Cent. Sci.* **2018**, *4*, 996–1006.
[7] P. Ertl, A. Schuffenhauer, *J. Cheminf.* **2009**, *1*, 8–18.
[8] V. Gutmann, *Coord. Chem. Rev.* **1976**, *18*, 225–255.
[9] a) L. Johnson, C. Li, Z. Liu, Y. Chen, S. A. Freunberger, P. C. Ashok, B. B. Praveen, K. Dholakia, J. M. Tarascon, P. G. Bruce, *Nat. Chem.* **2014**, *6*, 1091–1099; b) C. M. Burke, V. Pande, A. Khetan, V. Viswanathan, B. D. McCloskey, *Proc. Natl. Acad. Sci. USA* **2015**, *112*, 9293–9298; c) J. Chen, H. Zhang, M. Fang, C. Ke, S. Liu, J. Wang, *ACS Energy Lett.* **2023**, *8*, 1723–1734.
[10] a) Z. Li, H. Rao, R. Atwi, B. M. Sivakumar, B. Gwalani, S. Gray, K. S. Han, T. A. Everett, T. A. Ajantiwalay, V. Murugesan, N. N. Rajput, V. G. Pol, *Nat. Commun.* **2023**, *14*, 868–880; b) G. Zhang, J. Chang, L. Wang, J. Li, C. Wang, R. Wang, G. Shi, K. Yu, W. Huang, H. Zheng, T. Wu, Y. Deng, J. Lu, *Nat. Commun.* **2023**, *14*, 1081–1093; c) Y. Zhao, T. Zhou, M. Mensi, J. W. Choi, A. Coskun, *Nat. Commun.* **2023**, *14*, 299–308.
[11] a) R. Atwi, N. N. Rajput, *Patterns (N Y)* **2023**, *4*, 100799; b) Q. He, Y. Gorlin, M. U. M. Patel, H. A. Gasteiger, Y. C. Lu, *J. Electrochem. Soc.* **2018**, *165*, A4027–A4033.
[12] a) G. Bergerhoff, R. Hundt, R. Sievers, I. D. Brown, *J. Chem. Inf. Comput. Sci.* **1983**, *23*, 66–69; b) P. J. Linstrom, W. G. Mallard, *J. Chem. Eng. Data* **2001**, *46*, 1059–1063.
[13] T. Lu, Molclus program, Version 1.9.9.5., http://www.keinsci.com/research/molclus.html (accessed 1 August 2023).
[14] a) Y. Zhang, V. Viswanathan, *J. Phys. Chem. Lett.* **2021**, *12*, 5821–5828; b) O. Borodin, M. Olguin, C. E. Spear, K. W. Leiter, J. Knap, *Nanotech.* **2015**, *26*, 354003; c) Y. Okamoto, Y. Kubo, *ACS Omega* **2018**, *3*, 7868–7874.
[15] R. Stenutz, Gutmann Acceptor and Donor number, http://www.stenutz.eu/chem/solv21.php (accessed 1 August 2023).
[16] a) X. Fan, L. Chen, O. Borodin, X. Ji, J. Chen, S. Hou, T. Deng, J. Zheng, C. Yang, S. C. Liou, K. Amine, K. Xu, C. Wang, *Nat. Nanotechnol.* **2018**, *13*, 715–722; b) W. J. Xue, Z. Shi, M. J. Huang, S. T. Feng, C. Wang, F. Wang, J. Lopez, B. Qiao, G. Y. Xu, W. X. Zhang, Y. H. Dong, R. Gao, Y. Shao-Horn, J. A. Johnson, J. Li, *Energy Environ. Sci.* **2020**, *13*, 212–220.
[17] C. Cortes, V. Vapnik, *Mach. Learn.* **1995**, *20*, 273–297.
[18] J. H. Friedman, *Ann. Stat.* **2001**, *29*, 1189–1232.
[19] P. Geurts, D. Ernst, L. Wehenkel, *Mach. Learn.* **2006**, *63*, 3–42.
[20] J. Fürnkranz, in *Encyclopedia of Machine Learning* (Eds.: C. Sammut, G. I. Webb), Springer US, Boston, MA, **2010**, pp. 263–267.
[21] L. Breiman, *Mach. Learn.* **2001**, *45*, 5–32.

[22] N. S. Altman, *Am. Stat.* **1992**, *46*, 175–185.
[23] P. Sjoberg, J. S. Murray, T. Brinck, P. Politzer, *Can. J. Chem.* **1990**, *68*, 1440–1443.
[24] P. Politzer, J. S. Murray, F. A. Bulat, *J. Mol. Model.* **2010**, *16*, 1731–1742.
[25] J. R. Harding, C. V. Amanchukwu, P. T. Hammond, Y. Shao-Horn, *J. Phys. Chem. C* **2015**, *119*, 6947–6955.
[26] B. C. Ross, *PLoS One* **2014**, *9*, e87357.
[27] a) M. D. Bhatt, C. O'Dwyer, *Phys. Chem. Chem. Phys.* **2015**, *17*, 4799–4844; b) D. Y. Kim, M. S. Park, Y. Lim, Y.-S. Kang, J.-H. Park, S.-G. Doo, *J. Power Sources* **2015**, *288*, 393–400; c) Y. Wang, L. Xing, W. Li, D. Bedrov, *J. Phys. Chem. Lett.* **2013**, *4*, 3992–3999.
[28] Q. Q. Jia, Y. F. Ni, Z. T. Liu, X. Gu, Z. Y. Cui, M. T. Fan, Q. Zhu, Y. Wang, J. Ma, *J. Chem. Inf. Model.* **2022**, *62*, 4928–4936.
[29] Y. M. Gu, S. S. Tang, X. Liu, X. Y. Liang, Q. Zhu, H. F. Wu, X. Yang, W. H. Jin, H. W. Chen, C. Y. Liu, Y. Zhu, J. Ma, *J. Mater. Chem. A* **2024**, *12*, 4460–4472.
[30] Z. T. Liu, L. Q. Lin, Q. Q. Jia, Z. Cheng, Y. Y. Jiang, Y. W. Guo, J. Ma, *J. Chem. Inf. Model.* **2021**, *61*, 1066–1082.
[31] a) P. Winget, C. J. Cramer, D. G. Truhlar, *Theor. Chem. Acc.* **2004**, *112*, 217–227; b) A. V. Marenich, J. Ho, M. L. Coote, C. J. Cramer, D. G. Truhlar, *Phys. Chem. Chem. Phys.* **2014**, *16*, 15068–15106.
[32] *RDKit: Open-Source Cheminformatics Software (RRID: SCR 014274)*.
[33] H. A. Doan, G. Agarwal, H. Qian, M. J. Counihan, J. Rodriguez-Lopez, J. S. Moore, R. S. Assary, *Chem. Mater.* **2020**, *32*, 6338–6346.
[34] a) L. Xing, O. Borodin, G. D. Smith, W. Li, *J. Phys. Chem. A* **2011**, *115*, 13896–13905; b) P. Peljo, H. H. Girault, *Energy Environ. Sci.* **2018**, *11*, 2306–2309; c) J. Han, P. B. Balbuena, *Phys. Chem. Chem. Phys.* **2018**, *20*, 18811–18827.
[35] Z. Liu, T. Lu, Q. Chen, *Carbon* **2021**, *171*, 514–523.
[36] T. Brinck, J. S. Murray, P. Politzer, *Int. J. Quantum Chem.* **1993**, *48*, 73–88.
[37] T. Brinck, *J. Phys. Chem. A* **1997**, *101*, 3408–3415.
[38] R. T. Wrighta, K. Faya, A. Kennedya, K. Mayo-Beanb, K. Moran-Bruceb, W. Meylanc, P. Ranslowe, M. Lockc, J. V. Nabholzb, J. V. Runnenc, L. M. Cassidyc, J. Tunkeld, *ECOSAR v2.2 Class Program User's Guide* **2012**.

Manuscript received: December 14, 2024
Accepted manuscript online: February 10, 2025
Version of record online: February 25, 2025